Organic Geochemistry 181 (2023) 104604

Contents lists available at ScienceDirect

Organic Geochemistry

journal homepage: www.elsevier.com/locate/orggeochem

Climatic and environmentally driven variability in lacustrine brGDGT distributions at local to regional scales in Alaska and northwestern Canada

Gerard A. Otiniano [a,*], Trevor J. Porter [a], Rhys E. Buceta [a], Matthew E. Bergman [b], Michael A. Phillips [b]

[a] Department of Geography, Geomatics and Environment, University of Toronto - Mississauga, Mississauga, Ontario, Canada
[b] Department of Cells and Systems Biology, University of Toronto - Mississauga, Mississauga, Ontario, Canada

ARTICLE INFO

Associate Editor–**Isla S. Castaneda**

Keywords:
brGDGTs
Biomarker
Proxy
Lake
High-latitude
Subarctic
Arctic

ABSTRACT

Branched glycerol dialkyl glycerol tetraethers (brGDGTs) have attracted considerable interest from paleoclimate researchers due to their temperature sensitivity in modern environments, ubiquity, and preservation in the geologic record. BrGDGTs are especially attractive in high-latitude regions where the number of applicable proxies is limited. However, the climatic sensitivity of brGDGT assemblages varies between depositional environments and is uncharacterized for lacustrine systems in Alaska, Yukon, and Northwest Territories. This study addresses this knowledge gap by assessing the climate response of lacustrine brGDGTs from a network of lakes (n = 67) in Alaska and NW Canada (59.5 to 69.4° N). The mean temperatures of months of above freezing (MAF) are highly correlated with the fractional abundance of the IIIa brGDGT (Pearson's coefficient = -0.79, $p < 0.001$) as well as the methylation of branched tetraethers (MBT'_{5ME}) index (Pearson's coefficient = 0.75, $p < 0.001$) from Alaska, Yukon, and Northwest Territories. The fractional abundance of the IIIa brGDGT and the MBT'_{5ME} index are subsequently calibrated to climate using traditional ordinary least squares analysis and a user-friendly and open-source Bayesian regression analysis that yield comparable results. The climatic sensitivity of lacustrine brGDGTs in Alaska, Yukon, and Northwest Territories is unique in comparison to previously reported global assemblages and further varies between a subset of interior and coastal sites. The driver of this variability cannot yet be constrained, but future applications of brGDGTs as a paleoenvironmental proxy should select calibrations that closely resemble the past environment of interest. Wherever possible, paleoenvironments should be corroborated using independent proxies.

1. Introduction

Branched glycerol dialkyl glycerol tetraethers (brGDGTs; Sinninghe Damsté et al., 2000) offer insight into past climatic and environmental conditions from a wide variety of depositional environments and are quickly becoming a staple paleoclimate proxy (e.g., Bittner et al., 2022; Muñoz et al., 2020; Naafs et al., 2018; Peltier, 2015; Wang et al., 2018; Willard et al., 2019; Zhao et al., 2021). BrGDGTs are membrane lipids with a wide variety of chemical structures that are thought to be synthesized exclusively by bacteria (Weijers et al., 2006; Sinninghe Damsté et al., 2011, 2018; Chen et al., 2022; Halamka et al., 2022), which persist in the rock record over million-year timescales (e.g., Naafs et al., 2018; Otiniano et al., 2020). Moreover, brGDGTs are ubiquitous having been identified in a variety of environments spanning soils, peats, lakes, and marine environments (Weijers et al., 2007; De Jonge et al., 2014; Naafs et al., 2017b).

Past studies of brGDGTs relied on global datasets to derive empirical relationships between environmental conditions and the respondent relative distribution of brGDGT structures (e.g., De Jonge et al., 2014; Naafs et al., 2017b; Martínez-Sosa et al., 2021; Raberg et al., 2021; Véquaud et al., 2022). These relationships yielded climate reconstructions in agreement with independent analysis, which cumulatively support the reliability of brGDGTs as an archive of past conditions. The environmental dependence likely owes in part to bacteria physiology, as inferred from coherent trends between environmental conditions and novel brGDGT distributions (based on the degree of methylation and cyclization) across a global suite of brGDGT assemblages from twelve unique archives (Raberg et al., 2022b) as well as molecular dynamic simulations (Naafs et al., 2021) and bacterial culture studies (Chen et al., 2022; Halamka et al., 2022). However, persistent variations in environmental sensitivities at regional and local scales

* Corresponding author.
E-mail address: gerard.otiniano@mail.utoronto.ca (G.A. Otiniano).

https://doi.org/10.1016/j.orggeochem.2023.104604
Received 20 September 2022; Received in revised form 6 March 2023; Accepted 27 March 2023
Available online 30 March 2023

indicate additional factors also influence the temperature sensitivity of brGDGTs (Bechtel et al., 2010; De Jonge et al., 2019, 2021; van Bree et al., 2020). Although the source of this variation is unknown, significant attention has been paid to community effects wherein distinct assemblages of brGDGTs are produced in warm and cold regions (De Jonge et al., 2019). Moreover, brGDGT distributions in high-latitude regions may be biased towards warm season conditions (e.g., Naafs et al., 2017a; Cao et al., 2020; Raberg et al., 2021; Zhao et al., 2021), which is assumed to be driven by reduced bacterial activity under freezing (winter) conditions (e.g., Naafs et al., 2017a). Successful applications of brGDGTs to reconstruct past climate conditions in high-latitude regions indicate the regional applicability of this climate proxy; however, future applications would benefit from region-specific calibrations that reflect the unique depositional environment of interest. The focus of this study is to derive quantitative relationships between brGDGT distributions and climate in sub-Arctic and Arctic lakes in Alaska, Yukon, and Northwest Territories (AK-YK-NWT). Here we provide brGDGT assemblages from a suite of modern lake sediments from Alaska, Yukon, and Northwest Territories and compare them to modern climate parameters such as mean warm-season temperatures. The relationships between brGDGTs and modern climate conditions are explored via traditional and more-recently-developed regression techniques with consideration paid to geographical variations.

2. Methods

2.1. Study sites

Surface sediments from forty-three lakes were sampled in July of 2019. In Alaska, 6 lakes were sampled along the Richardson highway, ranging in latitude of 63.75° to 64.71°N, and elevation of 161–745 masl (Fig. 1). In Yukon and the Northwest Territories, thirty-seven samples were collected along the Klondike Highway, Dempster Highway, and the Inuvik-to-Tuktoyaktuk Highway, spanning 61.28° to 69.36° N, and elevation from 2 to 1187 masl. Top sediments (upper 5–10 cm below the sediment–water interface) were collected from the littoral zone of each lake, at ~ 30 cm water depth. The sediments were collected using a cleaned trowel, transferred to Whirlpack bags, and then kept in ice-cooled field coolers during fieldwork and later chilled to −20 °C at camp. The samples were shipped frozen to the University of Toronto, Mississauga, and remained frozen until they were processed. In addition to the samples collected in 2019, this dataset was supplemented with 24 previously published brGDGT samples (Fig. 1; Martínez-Sosa et al., 2021). The surface area of each lake was estimated from satellite imagery using Google Earth (earth.google.com/web/).

2.2. GDGT extraction and quantification

For each sample, a total lipid extract (TLE) was prepared from

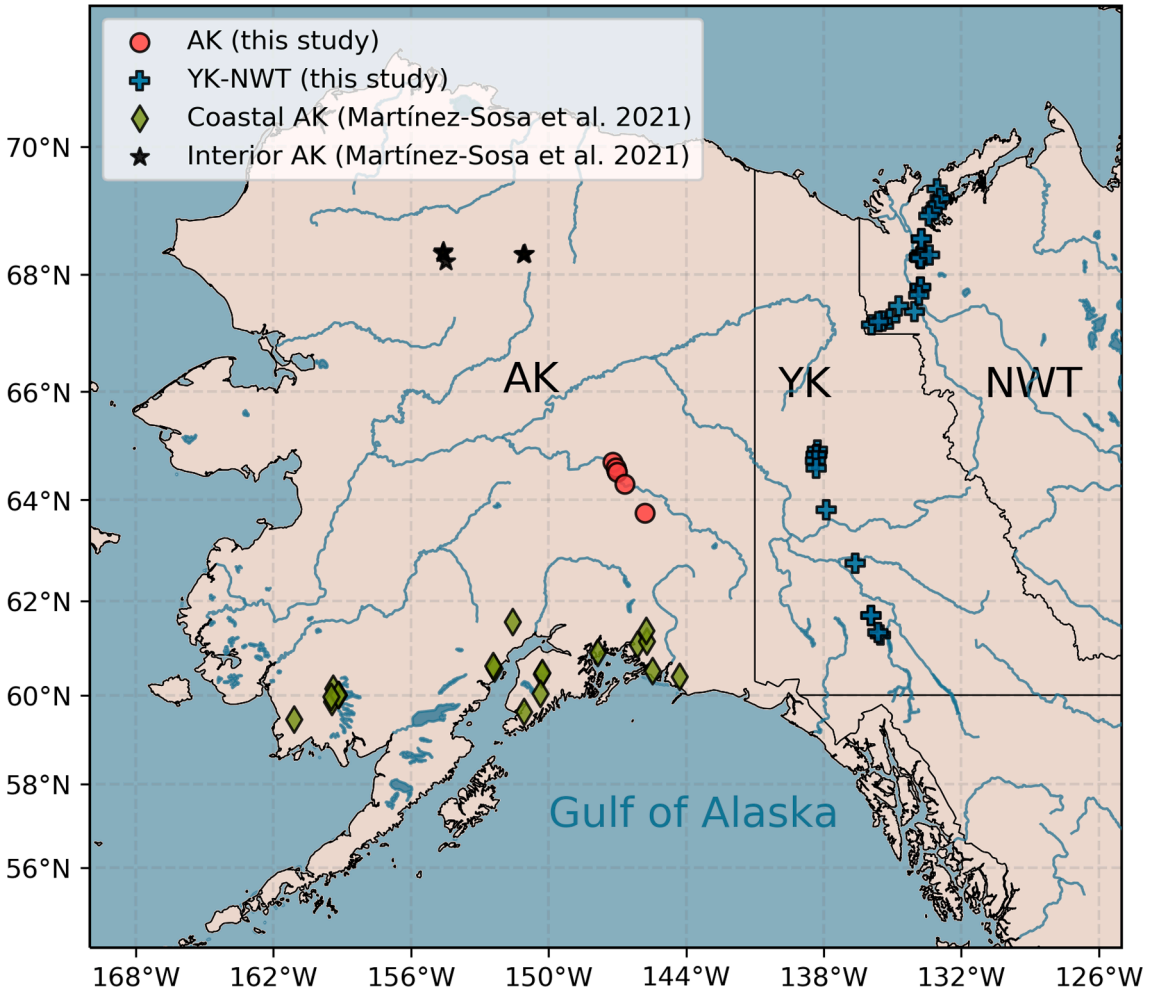

Fig. 1. Location of sampled lakes in Interior Alaska (red) and Interior Yukon (blue) as well as supplemental lakes from Coastal Alaska (yellow; Martínez-Sosa et al., 2021) and northern Alaska (black; Martínez-Sosa et al., 2021). (For interpretation of the references to colour in this figure legend, the reader is referred to the web version of this article.)

approximately 6 g lyophilized sediment by microwave assisted (Ethos Up Microwave) solvent extraction with 25 mL of 9:1 (v: v) dichloromethane (DCM): methanol (MeOH). The TLE was centrifuged at 3500 rpm for 15 min and then the supernatant was decanted. To ensure a maximized yield, the DCM: MeOH extraction was repeated twice more followed by centrifuging, and the TLE was then condensed under a gentle stream of high-purity dry nitrogen gas. The TLE was split into a polar and low-polarity or neutral fraction by column chromatography with an aminopropylsilyl-gel stationary phase packed in a 5.5-inch borosilicate pipette. The neutral fraction was eluted using a 2:1 (v: v) DCM: IPA mobile phase repeated three times, and the polar fraction was eluted with 4% formic acid in diethyl ether repeated three times. Both fractions were evaporated under nitrogen gas. The brGDGTs were isolated from the neutral fraction by column chromatography with a stationary phase of 5% water deactivated 100–200 mesh silica, and increasingly polar mobile phases of hexane, DCM, and MeOH, each repeated three times. The eluant was condensed under nitrogen gas and subsequently stored at −20 °C. Prior to analysis, the purified samples were brought to room temperature, dissolved in 99:1 (v: v) mixture of hexane: isopropanol, passed through a 0.45 μm PTFE membrane filter, and stored in autosampler vials.

BrGDGT targeted analysis was accomplished by ultra-high-performance liquid chromatography - mass spectrometry using an Agilent Technologies 1290 Series II UHPLC coupled to an AB Sciex 4500Q triple quadrupole mass spectrometer. Analytical conditions were based on Hopmans et al. (2016) and Otiniano et al. (2020). Briefly, the UHPLC was fitted with two 2.1 mm × 150 mm BEH HILIC (1.7 μm) columns connected in series. A 2.1 mm × 5 mm precolumn of the same sorbent was replaced regularly. Positive mode atmospheric pressure chemical ionization conditions were as follows: temperature 450 °C, ionization voltage +5500 V, nebulizer current of 3 μA, declustering potential +50 V. Data were acquired at unit resolution with a dwell time of 20 ms per ion. Quantification of brGDGTs was done by selected ion monitoring of $[M + H]^+$ quasimolecular ions at *m/z* 1018 (brGDGT-Ic), 1020, (brGDGT-Ib), 1022 (brGDGT-Ia), 1032 (brGDGT-IIc), 1034 (brGDGT-IIb), 1036 (brGDGT-IIa), 1046 (brGDGT-IIIc), 1048 (brGDGT-IIIb), and 1050 (brGDGT-IIIa).

2.3. GDGT indices

Fractional abundances of the individual brGDGT structures were used to calculate several environmentally sensitive indices defined by De Jonge et al. (2014) including the methylation of branched tetraethers (MBT'_{5ME}) index (Equation (1)), the cyclization of branched tetraethers (CBT') index (Equation (2)), and the isomer ratio (IR_{6ME}) index (Equation (3); Dang et al., 2016):

$$MBT'_{5ME} = \frac{Ia + Ib + Ic}{Ia + Ib + Ic + IIa + IIb + IIc + IIIa} \quad (1)$$

$$CBT' = log_{10}\frac{Ic + IIa' + IIb' + IIc' + IIIa' + IIIb' + IIIc'}{Ia + IIa + IIIa} \quad (2)$$

$$IR_{6me} = \frac{IIa' + IIb' + IIc' + IIIa' + IIIb' + IIIc'}{IIa + IIa' + IIb + IIb' + IIc + IIc' + IIIa + IIIa' + IIIb + IIIb' + IIIc + IIIc'} \quad (3)$$

Analysis of GDGT relative abundance, index calculations, and correlations to varying environmental and climatic variables were performed using Python 3.8.5 and the packages NumPy (Harris et al., 2020), Pandas (Reback et al., 2022), Math, and SciPy (Virtanen et al., 2020). A principal component analysis (PCA) using the Python scikit-learn 1.0.2 package was also carried out.

2.4. Bayesian modeling

The relationship between GDGT indices and climate parameters are investigated via frequentist and Bayesian methods. The former is approached with a traditional ordinary least squares (OLS) linear regression. The latter follows the dual-application of the Bayes rule (Tierney and Tingley, 2018), which has been employed in subsequent brGDGT calibrations (e.g., Dearing Crampton-Flood et al., 2020; Martínez-Sosa et al., 2021). The first application of the Bayes rule regresses environmental conditions against a brGDGT index, which yields an etiologically correct distribution of regression parameters. The posterior distributions of the regression parameters are then incorporated as priors into a second Bayes formula, which inverts the linear regression to estimate the initial predictor variable (e.g., temperature) from the initial responding variable (e.g., MBT'_{5ME}).

The previous instances of Bayesian regression techniques in the brGDGT community ultimately estimated the posterior predictive distributions of temperature associated with a given brGDGT parameter via a custom package, which incorporated a set of hard-coded prior distributions and sampling method (Gibbs sampler) for the first, and therefore second, implementation of the Bayes rule (Tierney and Tingley, 2018). In comparison, this study utilizes a more flexible approach to tune and calibrate brGDGT parameters to modern environmental conditions, wherein the user can more easily employ alternative sampling techniques and distributions. This degree of control is made possible by the comparatively user-friendly and open-source package, Bayesian Model-Building Interface (Bambi 0.90; Capretto et al., 2022), which sits atop the Bayesian statistical modelling package, PyMC (3.11.5; Salvatier et al., 2016). The PyMC packages offer a wide-variety of prior distributions and sampling techniques, the selection of which can be automated or specified via the user-friendly environment afforded by Bambi (Salvatier et al., 2016; Capretto et al., 2022). In combination, these packages offer users a uniquely accessible opportunity to explore and become familiar with the increasingly popular field of Bayesian analysis.

The etiologically correct regression of brGDGT assemblages and environmental conditions is configured through Bambi where the regression equation is defined using the observed and predictor variable (e.g., $MBT'_{5ME} \sim$ mean temperature of months above freezing; MAF). The associated prior distributions of the regression parameters (slope and intercept) are either user-dictated or can be automatically defined by Bambi. For this study, the slope is defined by a Gaussian distribution while the intercept is defined by a Gamma distribution given that brGDGT indices and fractional abundances must exist between 0 and 1. The mean and uncertainty parameters of these distributions are defined using the parameters from the initial OLS regression. The Bambi package recognizes the use of two variables as a linear regression and with the priors, outputs a model, which is then fitted to output a posterior distribution of the model parameters using a user-identified number of chains and draws via a sampling method configured by Bambi to best represent the data. The user then defines the inverse calculation of the linear model as a second formula and defines the associated model-priors using the estimated model-parameters from the first instance of the Bayes rule. A second model is then developed and fitted, again using the calibration dataset. From the posterior distribution of this fitted model, estimated MAF values are sampled to illustrate and assess the precision of the model. MAF values can be predicted from unknown

brGDGT samples by resampling the second model with model parameters dictated by the final calibration step. Access to the code utilized in this study is available on GitHub (https://github.com/GerardOtiniano).

2.5. Modern Climate

Modern climate conditions from high-latitude North America were calculated from the Copernicus Climate Change Service information 2021 using the ERA5 dataset from 1991 to 2020 (Copernicus Climate Change Service, 2019). The dataset included monthly temperatures (2 m above the surface) and precipitation (Muñoz-Sabater, 2021), which were obtained from the Climate Data Store on January 1, 2022. Across our study sites, mean annual temperatures range from −9.5 to −2.0 °C (mean −6.2 ± 2.9 °C) and mean annual precipitation ranges from 240 to 623 mm (mean 364 ± 91 mm). This data is accessible via the Polar Data Catalogue (https://doi.org/10.21963/13282). The MAF parameter was calculated by taking the average of all months above freezing between the years 1991 and 2020.

3. Results and Discussion

BrGDGTs were detected and quantified in forty-three samples from the interior Alaska, Yukon, and Northwest Territories dataset. A global calibration of lacustrine brGDGTs offer the opportunity to expand this dataset with surficial-lake-sediment samples from nineteen lakes in the coastal Alaska region in addition to five samples from the northern margin of the Brooks Range (Fig. 1). In combination, these data offer a total sample set of sixty-seven datapoints that cover a large portion of

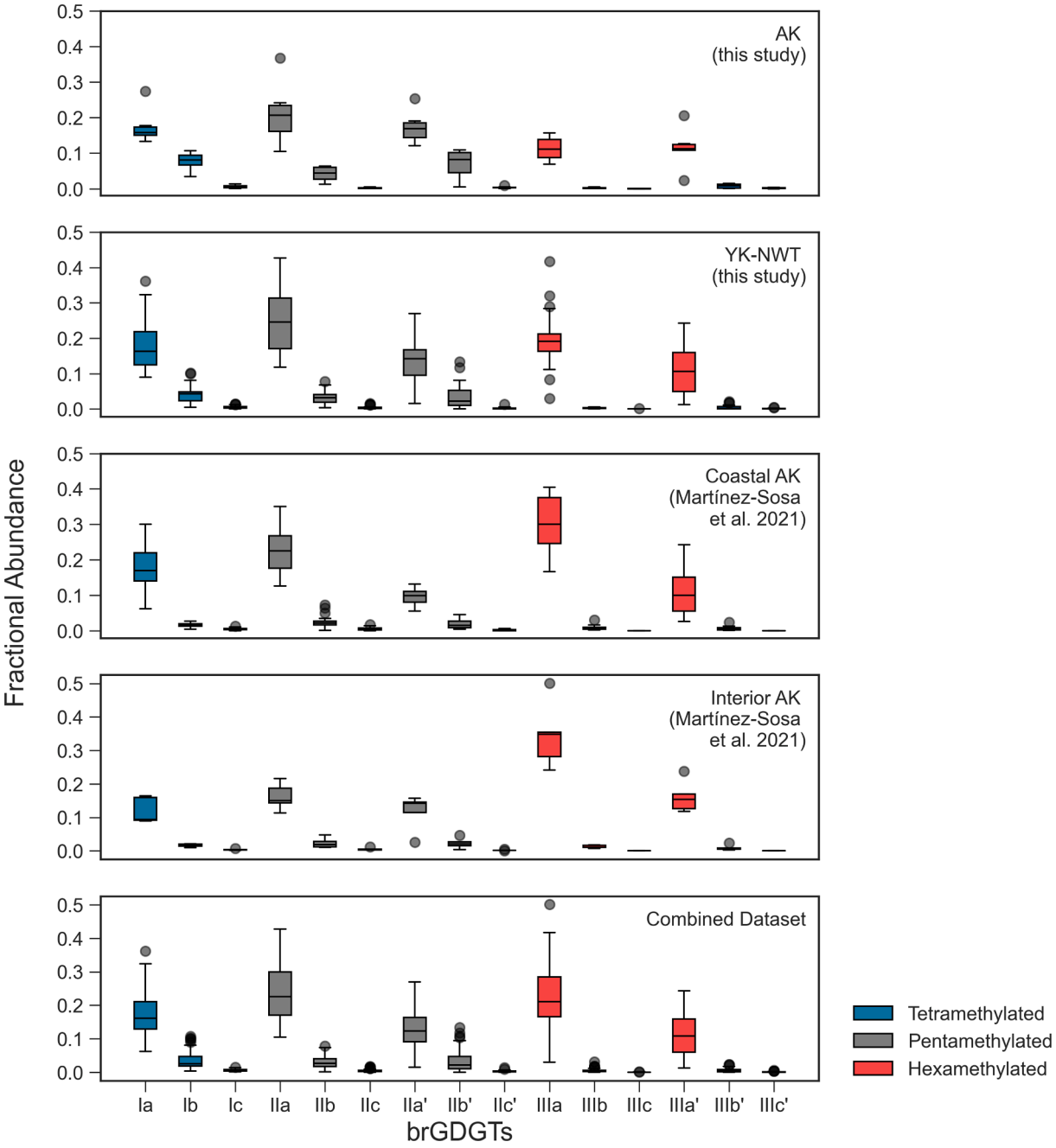

Fig. 2. The mean fractional abundance of the 15 brGDGT structures from (top to bottom) the interior Alaska sites (n = 6) and Yukon and Northwest Territories sites (n = 37) from this study, the coastal Alaska sites (n = 19) and interior Alaska sites (n = 5) from Martinez-Sosa et al. (2021), as well as the combined dataset (n = 67).

the northwestern North American Arctic region.

3.1. Regional brGDGT distributions and temperature sensitivity

Within the combined dataset, uncyclized brGDGTs are the most abundant structure. BrGDGT IIIa represents the greatest proportion of brGDGTs with a fractional abundance of 0.23 ± 0.1 (mean ± 2 σ), followed by IIa with a fractional abundance of 0.23 ± 0.08, and Ia with a fractional abundance of 0.17 ± 0.06 (Fig. 2). High relative abundances of uncyclized brGDGT structures are also observed in the greater-global lacustrine dataset (Martínez-Sosa et al., 2021), which includes a suite of 65 East African lake samples (Russell et al., 2018). Unlike the AK-YK-NWT dataset, however, the global dataset displays a greater abundance of brGDGT Ia (Martínez-Sosa et al., 2021). The differences in the fractional abundance of brGDGTs between the AK-YK-NWT dataset and the global dataset are to be expected given that higher Ia relative abundances are associated with higher temperatures just as higher IIIa fractional abundances are associated with lower temperatures (e.g., De Jonge et al., 2014).

Dimension reduction offers a clear illustration of the correlative relationships between brGDGT structures. A PCA of the combined brGDGT dataset yielded a first principal component that explains 44% of the variance within the data (Fig. 3) and is most dominantly influenced by positive loadings of penta- and hexa-methylated 6-methyl brGDGTs with one cyclopentane moiety (Table 1). Principal component two explains 19% of observed variability and is positively influenced by hexamethylated 5-methyl brGDGTs and negatively influenced by tetramethylated 5-methyl brGDGTs (Table 1).

We next carried out a direct gradient analysis of independent environmental variables to gain further insight into the distribution of brGDGT loadings within the PCA. The MAF parameter is described by a vector that plots in line with brGDGT IIIa (Fig. 3). The parallel relationship of these vectors infers a correlative relationship (Pearson's coefficient = -0.79, $p < 0.01$; Fig. 3). In contrast, the MAF vector plots orthogonal to brGDGTs IIa and Ia, which indicates a noncorrelative relationship (Pearson's coefficient = -0.02, $p = 0.87$ and Pearson's coefficient = 0.15, $p = 0.22$, respectively; Fig. 3). It is also important to consider the vector magnitude. For example, the magnitude of the MAF vector is larger than that of MAT, which indicates a comparatively stronger correlation to principal components one and two and therefore the dataset (Fig. 3).

The greater sensitivity of brGDGTs from the AK-YK-NWT dataset to

Table 1
BrGDGT loadings for components one and two form a principal component analysis performed in this study.

PC1		PC2	
brGDGT	Score	brGDGT	Score
IIb′	0.36	IIIa	0.49
IIIb′	0.34	IIIb	0.47
IIa	−0.34	Ib	−0.39
IIIa′	0.33	Ia	−0.29

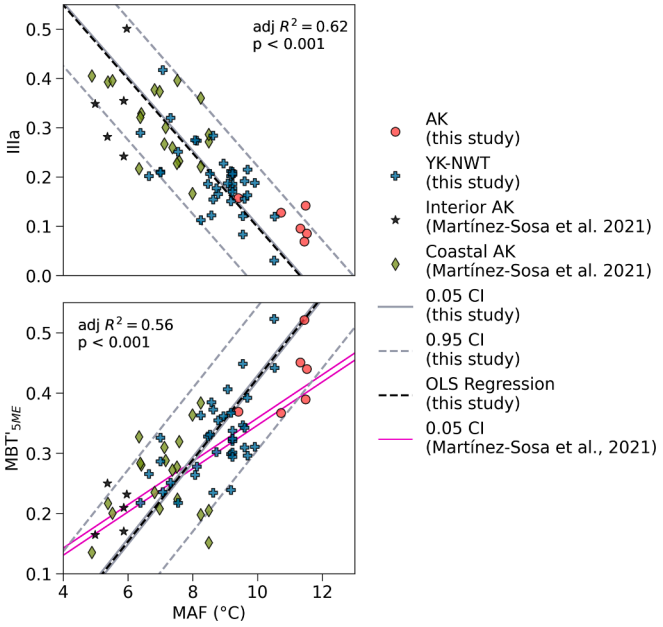

Fig. 4. AK-YK-NWT dataset displaying frequentist (black, dashed) and Bayesian linear regressions for the high-latitude lake dataset (grey, solid, 0.05 credible interval; grey, dashed, 0.95 credible interval). The similarity of the frequentist and Bayesian models result in overlap of the OLS regression line above the 0.05 CI. Also included is the recalibrated global dataset (0.5 credible interval, fuchsia; Martínez-Sosa et al., 2021) between MAF (°C), the fractional abundance of the IIIa brGDGT (left) and the MBT'_{5ME} index (right).

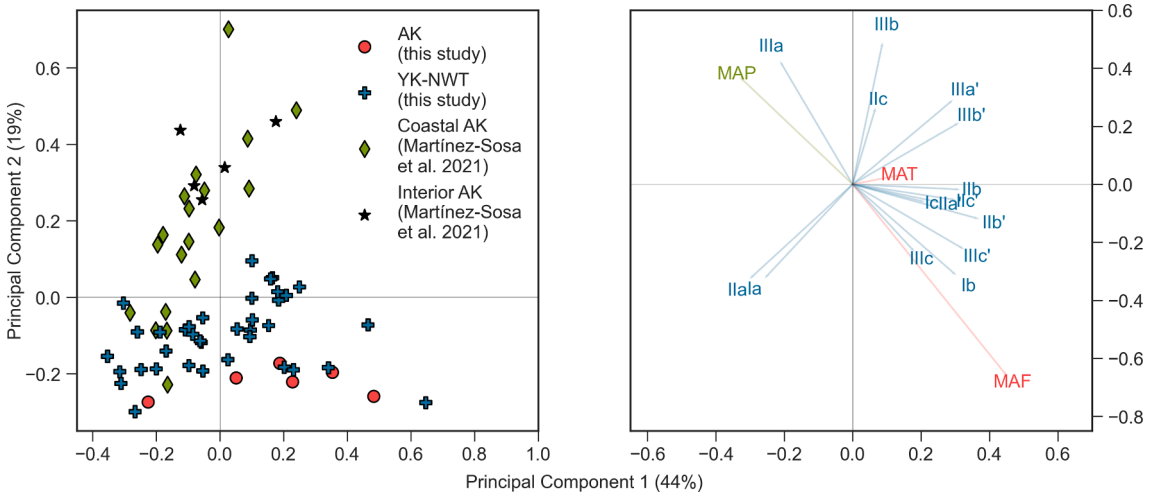

Fig. 3. Principal component analysis of the combined dataset displaying the score plot of regions for the first two components (left) and the loadings for the brGDGT and environmental variables (right), which include brGDGT structures (blue), mean annual precipitation (MAP, yellow), as well as mean annual temperatures (MAT) and mean monthly temperatures above freezing (MAF), (red). (For interpretation of the references to colour in this figure legend, the reader is referred to the web version of this article.)

warm-season temperatures relative to MAT is unsurprising given that winter months in high-latitude regions are below freezing temperatures, which should minimize brGDGT-producing bacterial activity and bias of the brGDGT record toward warm season temperatures (e.g., Naafs et al., 2017a). Indeed, a warm season bias is supported by previous reports of brGDGT distributions at high-latitudes and cold regions (Dang et al., 2018; Raberg et al., 2021; Zhao et al., 2021). Accordingly, brGDGTs from this study's complete network of lakes can be employed to reconstruct past warm season temperatures via mean temperature of months above freezing (MAF; Equation (4); Fig. 4).

$$\mathrm{MAF}(^{\circ}\mathrm{C}) = -13.29 \times \mathrm{IIIa} + 11.30 \quad (4)$$

($n = 67$, adj$R^2 = 0.62$, $p < 0.001$, RMSE 1.01 °C) where IIIa refers to the fractional abundance of the IIIa brGDGT.

The linear regression model for the AK-YK-NWT sites explains less variance, as interpreted from the adjusted coefficient of determination value, in comparison to previous global-scale studies by Martínez-Sosa et al. (2021; $R^2 = 0.85$) and Raberg et al. (2021; $R^2 = 0.91$). However, the comparatively high variance of the AK-YK-NWT dataset is typical of high-latitude regions (e.g., De Jonge et al., 2014; Dearing Crampton-Flood et al., 2020). In contrast, standard deviation of the prediction errors (RMSE) of the IIIa AK-YK-NWT model is low in comparison to previous models (e.g., Dang et al., 2018; Martínez-Sosa et al., 2021; Raberg et al., 2021; Russell et al., 2018) and further supports the applicability of the fractional abundance of the IIIa brGDGT as a high-latitude MAF temperature proxy.

The upper limit of MAF temperature sensitivity of the fractional abundance of IIIa, also identified by an absence of the IIIa brGDGT, is 11.6 °C. This dataset offers good coverage of the lower MAF limit (a minimum IIIa fractional abundance of 0.03), and the consistent linear behaviour of the IIIa-MAF relationship (Fig. 4) supports the applicability of a linear model for the full range of IIIa values reported here, from 0.03 to 0.32. In contrast, a theoretical sample composed entirely of brGDGT IIIa yields a lower MAF temperature limit of −2.8 °C, which contradicts the defined MAF parameter. It is possible that the irreconcilable lower temperature limit of this model owes to nonlinear behaviour of the IIIa brGDGT. For example, a global dataset of lacustrine brGDGTs yields an exponential relationship between MAF and the fractional abundance of global IIIa brGDGTs with respect to uncyclized brGDGTs (Raberg et al., 2021); however, the AK-YK-NWT are linearly distributed. Alternatively, a purely IIIa brGDGT distribution may not be possible. Indeed, a global distribution of lacustrine brGDGT distributions displays a maximum IIIa fractional abundance of 0.58 (Martínez-Sosa et al., 2021), while a composite dataset of high-latitude lakes in northeastern Canada and Iceland yields a maximum value of 0.62 (Raberg et al., 2021). In the context of the AK-YK-NWT calibration dataset, these maximum values equate to MAF temperatures of approximately 3.60 and 3.06 °C, respectively. However, no limiting factor to the production of the IIIa brGDGT has been identified. Further insight into the upper limit of brGDGT IIIa production would be made possible by additional sampling of high-latitude lakes under comparatively cooler conditions in this region. Until that time, the overall linearity of this calibration supports application of the MAF transfer function (Equation (4)) and any estimated MAF temperatures below 0 °C should be met with caution. Such scenarios would also benefit from the employment of an independent warm-season temperature proxy (e.g., pollen).

The temperature sensitivity of individual brGDGTs varies between the AK-YK-NWT dataset and the global lake dataset (Martinez-Sosa et al., 2021). For example, the global dataset displays an only moderately negative correlative relationship between temperature and brGDGT IIIa (Pearson's coefficient = 0.53) as well as brGDGT IIa (Pearson's coefficient = 0.3; Martínez-Sosa et al., 2021). Moreover, the global lake dataset displays a comparatively strong positive relationships between temperature and brGDGTs Ia (Pearson's coefficient = 0.57) and Ic (Pearson's coefficient = 0.48). Despite these differences, the global dataset and the AK-YK-NWT dataset display comparable regression parameters between MBT'_{5ME} and MAF temperatures (Fig. 4). As such, lacustrine brGDGTs offer a robust estimate of MAF conditions in the AK-YK-NWT region (Equation (5); Fig. 4).

$$\mathrm{MAF}(^{\circ}\mathrm{C}) = 14.75 \times \mathrm{MBT'_{5me}} + 3.74 \quad (5)$$

($n = 67$, adj$R^2 = 0.56$, $p < 0.001$, RMSE 1.16 °C).

The MBT'_{5ME}-MAF transfer function from the AK-YK-NWT dataset is associated with slightly smaller precision in comparison to that of the IIIa brGDGT calibration, as indicated by the slightly higher RMSE; however, this calibration offers a wider range of temperatures with a lower bound of 3.74 to 18.49 °C. Of particular interest is the smaller temperature range of both AK-YK-NWT calibrations in comparison to that of the global lacustrine calibration of MAF temperatures via the MBT'_{5ME} index, which spans 0 to 28.1 °C (Martínez-Sosa et al., 2021). The tighter range of predicable temperatures using the AK-YK-NWT MAF calibration likely owes to a suite of factors known to drive variability in brGDGT distributions (Section 3.3), such as microbial community changes (e.g., Chen et al., 2022) and lake water chemistry (e.g., Martínez-Sosa et al., 2021; Raberg et al., 2021; Halamka et al., 2022).

3.2. Bayesian regression analysis and model comparison

3.2.1. Validating open-source methods of Bayesian analysis

The proposed development of a Bayesian regression model using the Bambi and PyMC3 packages is validated by repeating the calibration and then comparing the validation parameters to the original global lake calibration (Martínez-Sosa et al. 2021). To maintain consistency, the original dataset and climate regression parameters are incorporated into the verification model (Fig. 4; Martínez-Sosa et al. 2021). Indeed, the coefficient of determination ($R^2 = 0.83$) and RMSE (2.6 °C) are comparable to those from the original calibration, 0.85 and 2.7 °C, respectively (Martínez-Sosa et al. 2021) and therefore validate the proposed open-access approach to Bayesian regression as an efficacious method of calibrating brGDGT indices to modern climate conditions.

The revised Bayesian calibration of high-latitude lacustrine IIIa and MBT'_{5ME} values against MAF offers comparable performance results to the OLS linear regression model, with adjusted R^2 values of 0.62 and 0.56, and RMSE values of 1.01 °C and 1.08 °C, respectively (Fig. 4; Fig. 5). Similarly, the IIIa-MAF and MBT'_{5ME}-MAF calibrations offer respective ranges of estimable MAF temperature from 0 to 11.30 ± 1.01 °C and 3.74 to 18.50 ± 1.08 °C, both of which are within error of the OLS calibration models.

The similar performance of the OLS and Bayesian methods do not suggest a superior method of regression analysis for calibrating brGDGTs to modern climate in this region. Moreover, both methods offer unique advantages such as the comparatively low-barrier-to-entry of the OLS regression and the ability to conduct etiologically correct regression via Bayesian analysis. Additional comparative analyses are needed to test this similarity in other regions and the open-source methods of Bayesian applications reported here will improve accessibility for these efforts.

3.2.2. Model comparison

The MBT'_{5ME} regression models from this study are of higher sensitivity in comparison to the global calibration model (Martínez-Sosa et al., 2021; Fig. 4) as interpreted from the comparatively steep slope of the AK-YK-NWT models. This relationship is also observed when plotting the actual MAF temperatures against the model-estimated temperatures (Fig. 5). For true MAF temperatures above ~ 8 °C, the MBT'_{5ME} and IIIa regression models produce values that are within error that are systematically underestimated (Fig. 5). For true MAF temperatures below 8 °C, the regression models yield values that are within error that are systematically overestimated (Fig. 5). This underestimation and overestimation of temperatures above and below ~ 8 °C is exaggerated by the Bayesian global lake calibration (Fig. 5). This finding is especially

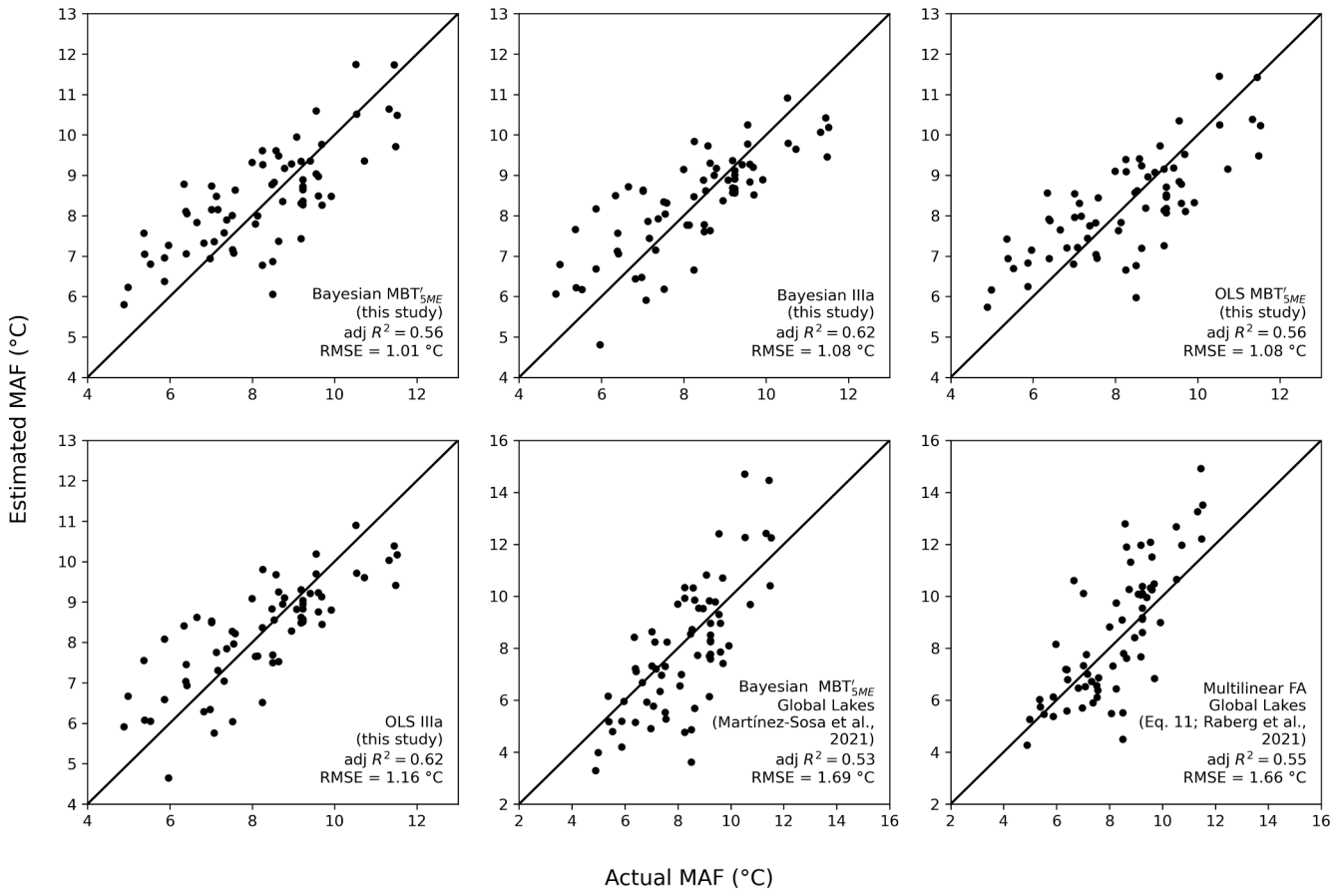

Fig 5. Comparison of actual and estimated MAF (°C) for each site in the AK-YK-NWT dataset using the Bayesian and OLS calibrations reported here, Bayesian MBT′$_{5ME}$ global lake calibration (Martínez-Sosa et al., 2021), and the multilinear fractional abundance (FA) calibration (Raberg et al., 2021).

noteworthy when considering that Bayesian regression analysis was initially employed in part to address regression attenuation observed in calibrations of brGDGTs (Naafs et al., 2017a; Dearing Crampton-Flood et al., 2020). The factors driving this perceived regression dilution and the subsequent underestimation of temperatures in high-latitude regions are yet to be identified but likely owe to multiple unconstrained factors (Section 3.3).

The fractional abundance of the IIIa brGDGT and the MBT′$_{5ME}$ index explains more variability than previous global calibrations of brGDGTs for the AK-YK-NWT brGDGT dataset (Fig. 5). In contrast, the MBT′$_{5ME}$ calibrations derived from the AK-YK-NWT explain a similar amount of variability relative to the Bayesian MBT′$_{5ME}$ global lake calibration (adjR^2 = 0.55, Fig. 5; Martínez-Sosa et al., 2021) and a multilinear fractional abundance calibration of brGDGTs differentiated by the degree of methylation and cyclization (Eq. 11, adj $R^2 = 0.55$; Raberg et al., 2021). However, the associated RMSEs of the Bayesian MBT′$_{5ME}$ global lake calibration (1.69 °C) and the multilinear fractional abundance calibration (1.66 °C) are both higher than the RMSE values associated with the AK-YK-NWT calibrations.

The similar adjusted coefficients of determination of the Bayesian MBT′$_{5ME}$ global lake calibration and the AK-YK-NWT calibrations support some global consistency of the index MBT′$_{5ME}$ to temperature in lacustrine datasets but the higher sensitivity of the fractional abundance of the IIIa brGDGT to MAF in the AK-YK-NWT illustrates geographic heterogeneities in this proxy. This heterogeneity of brGDGT distributions is further highlighted by the low correlation of the fractional abundance of the Ia brGDGT from the AK-YK-NWT dataset. In comparison, high-latitude and global calibrations of lacustrine brGDGTs typically report the fractional abundance calibration of the Ia brGDGT as the most sensitive brGDGT structure, with greater temperature sensitivity displayed by the MBT′$_{5ME}$ index (Martínez-Sosa et al., 2021; Raberg et al., 2021, 2022b; Zhao et al., 2021). Moreover, the tetramethylated fractional abundance of the Ia brGDGT (Ia_{Meth}; Raberg et al., 2021) also shows a weaker correlation with MAF (Pearson's coefficient 0.64, $p < 0.001$) relative to the fractional abundance of the IIIa brGDGT. As such, applications of the brGDGT climate proxy must employ calibrations that are environmentally analogous to environment of interest. Determining which environmental are important to this decision will be driven by future analysis of brGDGT-producing bacteria and variations in their response to environmental parameters.

3.2.3. *Model validation by application*

Assessment of a model's accuracy also typically involves its application to a previously published dataset. However, the scarcity of brGDGT-derived temperature records in the Alaska-Yukon region precludes a local application of the reported temperature calibrations. In

Table 2
Minimum, maximum, mean, and standard deviation values from the application of the reported OLS and Bayesian calibrations to a record of middle-Pleistocene brGDGT distributions (Lindberg et al., 2022).

	Ordinary Least Squares		Bayesian	
	IIIa (fractional abundance)	MBT′$_{5ME}$	IIIa (fractional abundance)	MBT′$_{5ME}$
Minimum (°C)	4.1	**5.5**	**4.4**	**5.5**
Maximum (°C)	**11.3**	**12.0**	**11.3**	**10.9**
Mean (°C)	**6.7**	**7.9**	**6.6**	**7.9**
Standard Deviation (2 σ)	**1.1**	**1.1**	**1.1**	**1.1**

place of local records, Lake El'gygytgyn, Siberia, offers the closest analogue to this study region given the relatively close proximity and similar modern climate and latitude (67.495 °N; Lindberg et al., 2022). The similarity of the Lake El'gygytgyn to the AK-YK-NWT region can be further justified by focusing on similar-to-modern intervals during tectonically recent periods such as the Pleistocene. Consequently, the OLS and Bayesian brGDGT climate calibrations are applied to a brGDGT record from Lake El'gygytgyn, from 1.00 to 1.15 Ma, a period of warmer-than-modern conditions (Lindberg et al., 2022).

In general, the OLS and Bayesian brGDGT calibrations yielded similar results for the subset of measured variables, the fractional abundance of the IIIa brGDGT and the MBT'_{5ME} index (Table 2). This similarity is expected given the comparable coefficient of determination and root-mean-square error values (Sections 3.1 and 3.2). Likewise, intercomparison of the models by indices demonstrates lower temperature estimates from the fractional abundance of the IIIa brGDGT in comparison to the MBT'_{5ME} index, which was anticipated by the lower slope of models that utilized the fractional abundance of the IIIa brGDGT (Table 2).

The AK-YK-NWT calibrations yield an oscillatory MAF trend, with warm periods coinciding with Marine Isotope Stages (MIS) 29, 31, and 33 (Fig. 6). Warmth during MIS31 is also reported by independent climate reconstructions of warm-season conditions from fossil pollen assemblages (Melles et al., 2012) and earlier applications of the brGDGT climate proxy (de Wet et al., 2016), which reported estimated temperatures in excess of 15 °C. However, such high temperature estimates are contentious with research suggesting that temperatures of Lake El'gygytgyn during this period should be more similar to the modern maximum of 5 to 6 °C (Lindberg et al., 2022). This line of reasoning led Lindberg et al. (2022) to select the global Bayesian brGDGT calibration as the most appropriate calibration for the middle-Pleistocene Lake El'gygytgyn record. As such, the coherence between lake El'gygytgyn temperature reconstructions derived from the global Bayesian calibration (Martínez-Sosa et al., 2021) and the four AK-YK-NWT lacustrine brGDGT calibrations supports the applicability of the OLS and Bayesian calibrations reported here.

3.3. Prospects from potential biases

3.3.1. Sources of brGDGTs

Efforts to characterize brGDGTs and the processes that influence their distributions in lacustrine environments often utilize sediment

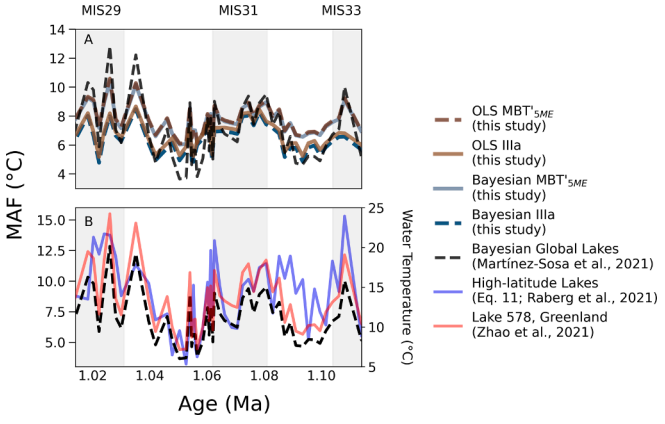

Fig 6. Estimated temperatures of Lake El'gygytgyn during the middle Pleistocene from brGDGTs during a subset of the 0.75 to 1.20 Ma record from Lindberg et al. (A; 2022) using the global Bayesian calibration (Martínez-Sosa et al., 2021) in comparison to the AK-YK-NWT Bayesian and OLS calibrations (A) as well as temperature estimates from the multilinear fractional abundance calibration (B, Eq. 11; Raberg et al., 2021) and lake-water temperatures estimated from the Lake 578, Greenland calibration (B, right axis; Zhao et al., 2021).

from the greatest lake-depths possible. Maximizing collection depth, and therefore the distance from soil-derived brGDGT reservoirs, should thereby offer the most pristine lake-brGDGT signal. This is important given observed differences in the sensitivity of brGDGTs to temperature in lake and soil sediments (Dang et al., 2018). Indeed, transects of suspended particulate within lakes have observed significant correlations of the MBT'_{5ME} index with depth, which is assumedly due to cooler in situ temperatures during brGDGT synthesis at depth (e.g., Stefanescu et al., 2021). In turn, some proportion of variability in brGDGT distributions from the littoral AK-YK-NWT dataset reported here likely owes to a mixed soil and lacustrine signal.

In the absence of a universal metric for determining the source environment of brGDGTs, past studies have leveraged the relative proportions of tetra-, penta-, and hexa-methylated to differentiate or identify similarities between lacustrine and soil brGDGT distributions (e.g., Russell et al., 2018; Kusch et al., 2019; Dearing Crampton-Flood et al., 2021). However, the efficacy of this brGDGT-source differentiation method to modern high-latitude soils and lake sediments is yet to be explored. The relative proportion of methylated brGDGTs from modern high latitude soils (Naafs et al., 2017a; De Jonge et al., 2019, 2021; Kusch et al., 2019; Dearing Crampton-Flood et al., 2020; Raberg et al., 2022b) overlap with brGDGT distributions from modern lake sediments in northeastern Canada and Iceland (Raberg et al., 2021), Greenland (Zhao et al., 2021), Alaska (Martínez-Sosa et al., 2021), and the littoral samples from the AK-YK-NWT dataset (Fig. 7). This overlap reflects the complexity of distinguishing lacustrine-derived brGDGTs from soil-derived brGDGTs, which likely owes in part to the contribution of soils to lake seidments via processes like surface runoff.

The ternary plot of tetra-, penta-, and hexa-methylated brGDGTs from soils show unique regional clusters. For example, a compilation of global brGDGT dsitributions in soils (Raberg et al., 2022b) from high-latitude (>55 °N) Russia and Svalbard (Naafs et al., 2017a; Kusch et al., 2019; Dearing Crampton-Flood et al., 2020) yield a unique cluster relative to high-latitude soils from Finland, Greenland, Iceland, Norway, Scotalnd, Sweden, and the USA (Naafs et al., 2017a; De Jonge et al., 2019, 2021; Dearing Crampton-Flood et al., 2020; Raberg et al., 2022b). Similarly, the littoral AK-YK-NWT dataset reported here indicates higher proportions of pentamethylated brGDGTs relative to the coastal and interior Alaskan lakes (Martínez-Sosa et al., 2021). Although this difference likely owes in part to differences in lake size as well as varrying soil contributions to both lacustrine brGDGT datasets, the similar regional difference in high-latitude soils indicate the potential significance of regionaly variable environmental conditions on brGDGT distirbutions.

Regional variations in brGDGT distirbutions from high-latitude lakes and soils are also illuminated using alternative, previously reported methods of brGDGT-source differentiation. For example, soil-derived brGDGTs are associated with a low ratio of uncyclized penta- to hexa-methylated brGDGTs (Σ IIIa / Σ IIa, < 0.59) in contrast to marine-derived brGDGTs, which are associated with high (>0.92) Σ IIIa / Σ IIa values (Xiao et al., 2016). These boundaries have also been applied in the differentiation of soil and aquatic production of brGDGTs archived in the sediments of Lake St Front, France (Martin et al., 2019). Soil-derived brGDGT distributions from Finland, Greenland, Iceland, Norway, Scotland, Sweden, and the USA (Naafs et al., 2017a; De Jonge et al., 2019, 2021; Dearing Crampton-Flood et al., 2020; Raberg et al., 2022b) yield expectedly low mean Σ IIIa / Σ IIa values of 0.33 ± 0.14. In comparison, a mean value of 0.90 ± 0.36 is observed in soils from Russia and Svalbard (Naafs et al., 2017a; Kusch et al., 2019; Dearing Crampton-Flood et al., 2020; Raberg et al., 2022b), which underscores the importance of regionally variable drivers of brGDGT distirbutions. Meanwhile, high-latitude lakes display comparatively consistent Σ IIIa / Σ IIa values. Lake 578, Greenland, yields a mean value of 1.03 ± 0.08 (Fig. SI; Zhao et al., 2021). Distributions of brGDGTs from lakes in Alaska and Iceland from the global Bayesian dataset (Fig. SI; Martínez-Sosa et al., 2021) yield a mean Σ IIIa / Σ IIa value of 1.49 ± 0.79 and

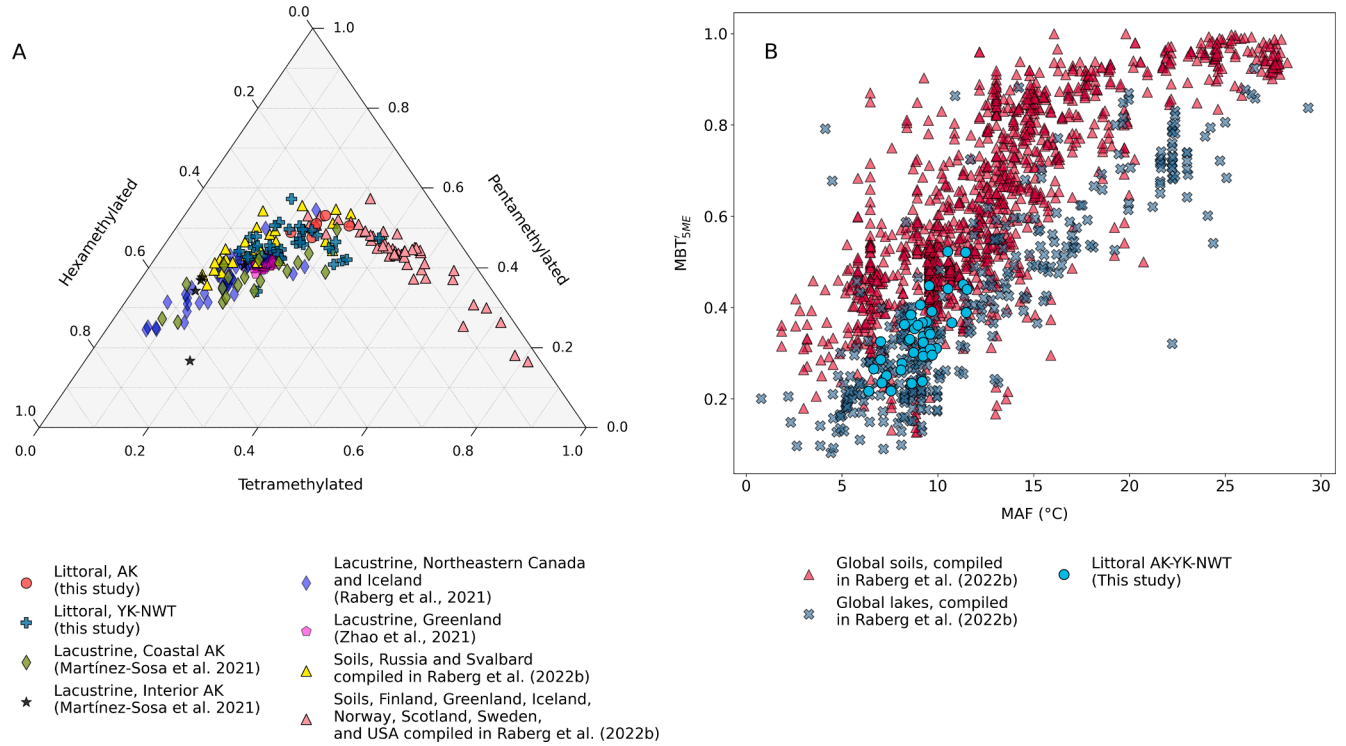

Fig. 7. A ternary diagram with axes indicating the proportion of tetra, penta, and hexamethylated brGDGTs from the AK-YK-NWT dataset (this study), high-latitude (>55 °N) lakes from northeastern Canada and Iceland (Raberg et al., 2021), Lake El'gygytgyn (Lindberg et al., 2022); Lake 578, Greenland (Zhao et al., 2021) and high-latitude (>55°N) soils from Russia and Svalbard as well as Finland, Greenland, Iceland, Norway, Scotland, Sweden, and the USA, as compiled in Raberg et al. (2022b) (A). A biplot of MAF (°C) and MBT'_{5ME} values illustrates the temperature response of brGDGTs from the littoral AK-YK-NWT dataset and modern soils (red triangle) and lake sediments (blue x's), as compiled in Raberg et al. (2022b) (B). (For interpretation of the references to colour in this figure legend, the reader is referred to the web version of this article.)

high-latitude Canadian and Icelandic lakes yield a mean value of 1.53 ± 0.61 (Fig. SI; Raberg et al., 2021). In comparison, brGDGT distributions from the AK-YK-NWT dataset yield a lower mean Σ IIIa / Σ IIa value of 0.79 ± 0.24 (Fig. SI), which supports the assumption that soils contribute to the littoral AK-YK-NWT dataset.

The proportion of soil to lake-derived brGDGTs cannot be quantified without brGDGT distributions from local soils and deep-lake sediments. In contrast, a qualitative comparison of the temperature-driven response of soil-derived brGDGTs and lake-derived brGDGTs suggests that AK-YK-NWT dataset is dominated by lake-derived brGDGTs. This is best illustrated by comparing the temperature sensitivities of MBT'_{5ME} values of global soil and lacustrine datasets (Fig. 7). Typically, MBT'_{5ME} values from soils are calibrated to MAT. However, global soil-derived MBT'_{5ME} values (Raberg et al., 2022b) also show a significant linear relationship with MAF (Fig. 7; Pearson's coefficient 0.79, $p < 0.001$) derived from ERA5 reanalysis data (Copernicus Climate Change Service, 2019; Muñoz-Sabater, 2021), which permits a comparison of MBT'_{5ME} temperature dependence from soils and lakes (Fig. 7; Raberg et al., 2022b). Soil derived MBT'_{5ME} values are typically higher than MBT'_{5ME} values for any given MAF value (Fig. 7), which suggests that lacustrine calibrations should overestimate MAF from soil-derived brGDGT distributions. In contrast, the AK-YK-NWT dataset are accurately estimated using independent lake calibrations of MBT'_{5ME} to MAF and therefore indicate a dominant lacustrine source of brGDGTs from the AK-YK-NWT dataset (Fig. 7). A more definitive understanding of brGDGT provenance from the AK-YK-NWT dataset requires future characterization of soil and deep-lake sediment from this region. Future research that focuses on the signal captured by shallow lake sediments would also provide immense benefit to paleoclimate reconstruction efforts that rely on paleo-lacustrine deposits. Regions such as central Alaska and Yukon offer paleo-lake sediments that date to the late Miocene, but determining the paleodepth of these deposits is not always possible (Otiniano et al., 2020).

Future analysis of littoral brGDGT distributions should incorporate additional biomarkers to help assess the contribution of soil-derived brGDGTs. For example, the source of brGDGT assemblages in arctic lake catchments were differentiated by a high abundance of intact brGDGTs with monoglycosyl head groups while lacustrine brGDGTs were associated with the dominance of phosphohexose brGDGTs (Raberg et al., 2022a). The proportion of soil-derived brGDGTs has also been constrained in shallow lacustrine sediments by measuring the concentrations of long chain C_{33} *n*-alkanes and the isoprenoidal GDGTs crenarchaeol and crenarchaeol′ (Wang et al., 2023). Notably, Wang and others (2023) observed low (<10%) contributions of soil-derived brGDGTs. Future studies that test these methods in the AK-YK-NWT region would aid in our understanding of brGDGT sources and elucidate potential drivers of the apparent regional variations in brGDGT assemblages.

Sampling littoral brGDGT assemblages offers unique advantages to deep lake sediments. For example, shallow lake sediments circumvent complications such as deep-lacustrine anoxia at depth, which is known to drive brGDGT methylation of the brGDGT-producing Acidobacterium *Solibacter usitatus* (Halamka et al., 2022). Indeed brGDGT production throughout the water column varies with oxygen content, which can therefore complicate the interpretation of brGDGT records from stratified lakes (e.g., Weber et al., 2018; van Bree et al., 2020). Regardless, further assessment of the environmental sensitivity of brGDGT distributions in shallow lake sediments is needed to fully appreciate the potential of brGDGTs as an archive of past climate.

3.3.2. *Other influences on brGDGT variability*

Although many of the influences on brGDGT distributions will likely remain hidden until additional strains of brGDGT-producing bacteria are discovered (e.g., Chen et al., 2022), some sources of uncertainty can be identified and addressed. For example, calibrations of lake-derived

brGDGTs commonly employ modelled air temperatures in lieu of water temperatures, which contributes to the apparent warm bias (Cao et al., 2020; Raberg et al., 2021). Within this framework, the smaller lakes of the littoral AK-YK-NWT dataset likely warm quicker and to a higher temperature than the larger and deeper lakes of the itnerior and coastal Alaskan sites (Martínez-Sosa et al., 2021). As such, brGDGTs synthesize in the littoral zone reflect a smaller bias between air temperature and water, which could partially explain the higher sensitivity of MAF-MBT′$_{5ME}$ calibrations from the AK-YK-NWT dataset relative to the Bayesian global lake calribation (Martínez-Sosa et al., 2021). However, biases such as this are difficult to constrain as continuous temperature measurements from appropriate lake-depths are difficult to coordinate and require further comparison of brGDGT distributions from shallow and deep-water lakes in this region.

Biases related to physical and chemical processes of the lake can be accounted for with additional sampling. For example, analysis of dissolved oxygen in a lake may prove beneficial as different regimes of dissolved oxygen content in lake water drives distinct bacterial communities, which yield distinct brGDGT distributions (Weber et al., 2018; Cao et al., 2020; Wu et al., 2021). However, In high-latitudes, the influence of seasonal anoxia as a result of restricted air–water interactions from lake ice (e.g., Raberg et al., 2021), may act as another driver of the apparent warm season bias (Cao et al., 2020). Moreover, anoxia is an unlikely driver of variability in the littoral sediments of the AK-YK-NWT dataset.

Other aspects of water chemistry, such as conductivity, also have influences on brGDGT distributions (e.g., Martínez-Sosa et al., 2021; Raberg et al., 2021). Similarly, soils of variable cation exchange capacities along a Scandinavian altitudinal transect display variable associated temperature sensitives of brGDGTs (Halffman et al., 2022). However, we are unable to estimate or account for the influence of these properties on the brGDGTs from AK-YK-NWT without the associated data. Future analysis of these properties will likely aid in explaining variability that is unattributable to climate.

3.4. Other environmental influences, the community effect, and subregional patterns

The correlative relationships between brGDGT structures throughout AK-YK-NWT with MAP mirrors those between the brGDGTs and MAF conditions, which are inferred from the oppositely oriented MAP and MAF vectors from the gradational analysis (Fig. 3). However, the former relationships are comparatively weaker than the latter. For example, MAP is most strongly correlated to IIIa with a Pearson's coefficient of 0.50 ($p < 0.001$). A similar trend is observed between MAP and brGDGT indices that previous studies typically calibrate to environmental parameters other than temperature, such as CBT′ with pH (e.g., De Jonge et al., 2014; Dearing Crampton-Flood et al., 2020). Here the CBT′ index ranges from −1.44 to 0.26 (mean −0.40) and only weaky correlates with MAP (Pearson's coefficient −0.28, $p = 0.02$; Fig. 8). Alternatively, these trends could be driven by a gradient of conductivity between the lakes as conductivity is known to correlate with MAP and IR$_{6ME}$ (Martínez-Sosa et al., 2021). Future analysis of water conductivity and brGDGTs in these regions are needed to begin determining the driver of this trend.

The MAP and CBT′ data are heteroscedastic with greater variance in CBT′ when MAP is below 1000 mm per year, and with comparatively less variance when MAP is>1000 mm per year (Fig. 8). The cause of this trend in variation is best explained by the location of brGDGT synthesis, wherein, sites north of the Alaska Range, referred to as interior sites, are characterized by dry conditions with mean MAP of 402 ± 108 mm, which does not significantly correlate with the associated CBT′ ($p = 0.07$; Fig. 8) and IR$_{6ME}$ ($p = 0.09$; Fig. 8) indices. Meanwhile, sites from the Gulf Coast of Alaska are characterized by wetter conditions with a mean MAP of 1831 ± 795 mm which do significantly correlate with the CBT′ (Pearson's coefficient = -0.65, $p = 0.003$; Fig. 8), IR$_{6ME}$ (Pearson's coefficient = -0.65, $p = 0.003$; Fig. 8) and IIa′ brGDGT indices (Pearson's coefficient = -0.66, $p = 0.02$; Fig. 8).

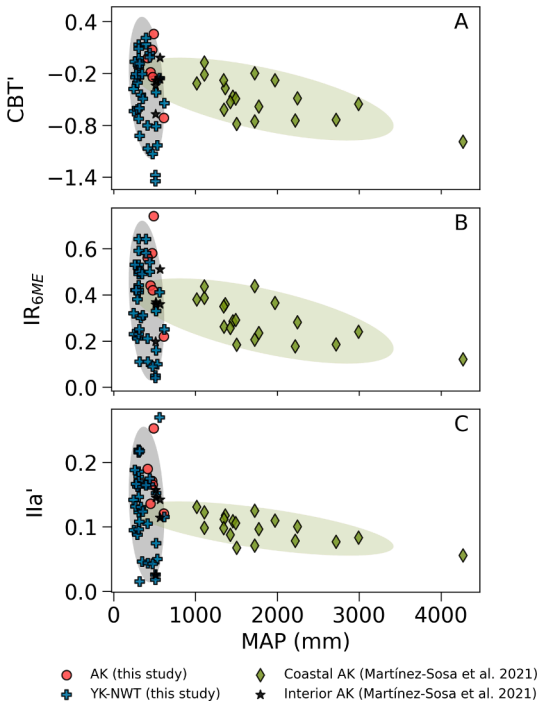

Fig. 8. Biplots of MAP with the indices CBT′ (A), IR$_{6ME}$ (B) and the fractional abundance of brGDGT IIa′ **(C)** using brGDGT assemblages from interior AK-YK-NWT (black ellipse, 95% confidence interval) and coastal Alaska sites (yellow ellipse, 95% confidence interval; Martínez-Sosa et al., 2021). (For interpretation of the references to colour in this figure legend, the reader is referred to the web version of this article.)

Although it is not-yet possible to determine what factor drives the geographically asymmetric sensitivity of brGDGT assemblages to MAP (Fig. 8), one possible explanation may involve a bacterial community effect. Alternatively, this phenomenon could reflect terrestrial contributions of brGDGTs into the coastal lacustrine sites. Shallow lake-sediments are susceptible to surface processes and may incorporate terrestrial material while benthic lacustrine sediments are comparatively decoupled from surface processes (Weber et al., 2018). Moreover, precipitation-dependent brGDGT assemblage have been inferred from an indirect relationship of IR$_{6ME}$ on MAP via pH in subtropical Chinese soils (Wang et al., 2018). A similar observation of CBT′$_{5ME}$ values varying with precipitation amounts was observed in brGDGT assemblages from soils northern Iran (Duan et al., 2022). As such, the potential uncertainty of terrestrial inputs into shallow lake sediments is incorporated into the lacustrine brGDGT calibration reported here. The incorporation of this uncertainty is significant as paleodepths are often inestimable from of Neogene lacustrine deposits in this region.

The geographically-variable sensitivity of brGDGT assemblages to climate conditions in the AK-YK-NWT dataset is comparable to a difference in temperature sensitivity of brGDGTs collected from different thermal regimes at the ForHot research site in Iceland (De Jonge et al., 2019). The measured brGDGTs distributions displayed a distinct change in bacterial community when temperatures increased above 14 °C (De Jonge et al., 2019). These hot (>14 °C) and cold (<14 °C) distinctions were then applied to a global-distribution of soils, from which hot- and cold-derived brGDGTs produced discrete sensitivities to temperature and pH (De Jonge et al., 2019, 2021). A similar phenomenon has also been observed in lakes where seasonal variations in brGDGT distributions better reflect changes in bacterial communities in comparison to the local environment (Bechtel et al., 2010; van Bree et al., 2020). Additional field observations (Russell et al., 2018) and laboratory incubations (Martínez-Sosa et al., 2020) of lake waters have also inferred

Table 3
A summary of the monthly temperatures that best correlate with the fractional abundance of the IIIa brGDGT or the MBT'_{5ME} index in lakes from Coastal Alaska and interior AK-YK-NWT.

Location (Number of samples)	brGDGT parameter	Temperature regime (Pearson's coefficient, p)
Coastal Alaska	IIIa	July (-0.53, 0.02)
(19)	MBT'_{5ME}	None
Interior AK-YK-NWT	IIIa	October (-0.81, <0.001)
(44)	MBT'_{5ME}	June (-0.82, <0.001)

an influence of bacterial community changes on brGDGT distributions from positive correlations between the IR_{6ME} index and temperature. As such, a yet unidentified driver of bacterial communities could be responsible for the differential climate responses observed form lacustrine brGDGTs from in interior AK-YK-NWT and from the coastal Alaskan region.

The factor(s) that bear responsibility for driving the differentiated MAP sensitivity of lacustrine brGDGTs from interior AK-YK-NWT and coastal Alaska may also manifest as a comparatively weak temperature sensitivity in the coastal region. The coastal sites (n = 19) display a correlation between the IIIa brGDGT and July temperatures (Pearson's coefficient −0.53, $p = 0.02$; Table 3) while the MBT'_{5ME} index does not significantly correlate ($p > 0.05$; Table 3) with any temperature regime. The reduced temperature-brGDGT correlation likely owes, at least in part, to the region's narrower range in annual temperatures (21.88 °C) in comparison to that of the total dataset (33.02 °C). From the interior AK-YK-NWT region, the MBT'_{5ME} best correlates with June temperatures (Pearson's coefficient = -0.82, $p < 0.001$; Table 3), which is unsurprising given the high correlation between MAF and June temperatures (Pearson's coefficient = 0.96, $p < 0.001$). In contrast, the fractional abundance of the IIIa brGDGT from interior lakes best correlates with October temperatures (Pearson's coefficient = -0.81, $p < 0.001$; Table 3), which share a comparatively weak correlation with MAF (Pearson's coefficient = 0.59, p = 0.007). It is unlikely that the brGDGT-producing bacteria are directly responding to October temperatures (mean = -5.10 ± 3.72 °C) given an assumed reduction of productivity when ambient temperatures are below-freezing (e.g., Naafs et al., 2017a). Instead, the shift in temperature-sensitivity likely reflects a yet unidentified environmental parameter that biases the relative abundance of IIIa brGDGTs in accordance with October temperatures. Regardless of this driver, the seasonal sensitivity of the IIIa brGDGT reflects the potential for regional variations in the climatic and environmental sensitivity of brGDGTs, which must be considered when employing brGDGTs as a tool for paleoclimate and paleoenvironmental reconstructions.

4. Conclusion

BrGDGT distributions from the littoral zone of small high-latitude lake in Alaska and northwestern Canada most closely correlate with MAF, which agrees with previous investigations. However, previous studies found the MBT'_{5ME} index to best correlate with temperature while the AK-YK-NWT produces a maximum correlation between temperature and the fractional abundance of the IIIa brGDGT. Moreover, the MBT'_{5ME} index from lakes in AK-YK-NWT is more sensitive to changes in MAF in comparison to global brGDGT behaviour. Differences between the distributions of brGDGTs from the AK-YK-NWT dataset and other lake studies may owe to multiple factors that include lake size as well as hydrological and chemical influences. Soil-derived brGDGTs are likely incorporated in AK-YK-NWT dataset. However, soil contributions are likely low as the littoral AK-YK-NWT dataset yields an overall MBT'_{5ME}-MAF distribution that is more consistent with a global compilation of lakes than soils. Future studies comparing brGDGT distributions from soils and maximum lake depths in this region are needed to better constrain the amount of soil-derived brGDGTs that may be incorporated into these samples. Unique brGDGT sensitivity from the AK-YK-NWT dataset is also observed at the sub-regional scale where CBT′ and IR_{6ME} index values highly correlate with MAP in lakes from coastal Alaska, which is not observed for the interior AK-YK-NWT sites. Similarly, coastal Alaskan sites show weak correlation between the fractional abundance of the IIIa brGDGT and temperature and no relationship between MBT'_{5ME} and temperature. In comparison, the interior AK-YK-NWT sites yield high correlations between the fractional abundance of the IIIa brGDGT and October temperatures. The cause of this geographic variation in brGDGT sensitivity is unidentified, but similar observations of brGDGT behaviour point to regionally variable bacterial communities as a potential driver. As such, future employment of brGDGTs as a paleoclimate or paleoenvironmental proxy should ensure the employed calibrations best reflect the paleo-environment of interest. Environmental context could be ascertained using additional geochemical archives of past conditions such as pollen or fossil leaf waxes.

This study further explored the brGDGT-climate relationship via traditional OLS and Bayesian regression methods, which yielded concordant model-validation metrics and therefore supports the use of either regression technique as valid approach to calibrating brGDGTs. Moreover, the presented user-friendly method of Bayesian regression model derivation using open-source packages in the Python environment offers an accessible entrance into Bayesian analysis techniques for those interested.

Data Availability Statement.

The brGDGT and modern climate data that was collected by the authors in 2019 can be downloaded from the Polar Data Catalogue (https://doi.org/10.21963/13282).

Declaration of Competing Interest

The authors declare that they have no known competing financial interests or personal relationships that could have appeared to influence the work reported in this paper.

Data availability

The data is available as a Supplementary Data file and at the Polar Data Catalogue (https://doi.org/10.21963/13282).

Acknowledgements

The authors acknowledge funding provided by NSERC Discovery Grants to TP (RGPIN-2016-06730) and MP (RGPIN-2017-06400) and infrastructure funding from the Canadian Foundation for Innovation-Ontario Research Fund John Evans Leaders Fund to TP (Project # 34864) and MP (Project # 36131). We thank KH and SB for field assistance as well as AT, JF, and FN for their assistance in the lab. The authors also express gratitude towards the executive editor of Organic Geochemistry, Dr. Isla Castañeda, as well as Jonathan Raberg, and the two anonymous reviewers who provided insightful and constructive comments that aided in our appreciation and communication of this work.

Appendix A. Supplementary material

Supplementary data to this article can be found online at https://doi.org/10.1016/j.orggeochem.2023.104604.

References

Bechtel, A., Smittenberg, R.H., Bernasconi, S.M., Schubert, C.J., 2010. Distribution of branched and isoprenoid tetraether lipids in an oligotrophic and a eutrophic Swiss lake: Insights into sources and GDGT-based proxies. Organic Geochemistry 41, 822–832.

Bittner, L., De Jonge, C., Gil-Romera, G., Lamb, H.F., Russell, J.M., Zech, M., 2022. A Holocene temperature (brGDGT) record from Garba Guracha, a high-altitude lake in Ethiopia. Biogeoscience 19, 5257–5374.
Cao, J., Rao, Z., Shi, F., Jia, G., 2020. Ice formation on lake surfaces in winter causes warm-season bias of lacustrine brGDGT temperature estimates. Biogeosciences 17, 2521–2536.
Capretto, T., Piho, C., Kumar, R., Westfall, J., Yarkoni, T., Martin, O.A., 2022. Bambi: A simple interface for fitting Bayesian linear models in Python. Journal of Statistical Software 103, 1–29.
Chen, Y., Zheng, F., Yang, H., Yang, W., Wu, R., Liu, X., Liang, H., Chen, H., Pei, H., Zhang, C., Pancost, R.D., Zeng, Z., 2022. The production of diverse brGDGTs by an Acidobacterium allows a direct test of temperature and pH controls on their distribution. bioRxiv. https://doi.org/10.1101/2022.04.07.487437.
Copernicus Climate Change Service, 2019. ERA5 monthly averaged data on single levels from 1979 to present. doi:10.24381/CDS.F17050D7.
Dang, X., Ding, W., Yang, H., Pancost, R.D., Naafs, B.D.A., Xue, J., Lin, X., Lu, J., Xie, S., 2018. Different temperature dependence of the bacterial brGDGT isomers in 35 Chinese lake sediments compared to that in soils. Organic Geochemistry 119, 72–79.
Dang, X., Yang, H., Naafs, B.D.A., Pancost, R.D., Xie, S., 2016. Evidence of moisture control on the methylation of branched glycerol dialkyl glycerol tetraethers in semi-arid and arid soils. Geochimica et Cosmochimica Acta 189, 24–36.
De Jonge, C., Hopmans, E.C., Zell, C.I., Kim, J.-H., Schouten, S., Sinninghe Damsté, J.S., 2014. Occurrence and abundance of 6-methyl branched glycerol dialkyl glycerol tetraethers in soils: Implications for palaeoclimate reconstruction. Geochimica et Cosmochimica Acta 141, 97–112.
De Jonge, C., Kuramae, E.E., Radujković, D., Weedon, J.T., Janssens, I.A., Peterse, F., 2021. The influence of soil chemistry on branched tetraether lipids in mid- and high latitude soils: implications for brGDGT- based paleothermometry. Geochimica et Cosmochimica Acta S310, 95–112.
De Jonge, C., Radujković, D., Sigurdsson, B.D., Weedon, J.T., Janssens, I., Peterse, F., 2019. Lipid biomarker temperature proxy responds to abrupt shift in the bacterial community composition in geothermally heated soils. Organic Geochemistry 137, 103897.
de Wet, G.A., Castañeda, I.S., DeConto, R.M., Brigham-Grette, J., 2016. A high-resolution mid-Pleistocene temperature record from Arctic Lake El'gygytgyn: a 50 kyr super interglacial from MIS 33 to MIS 31? Earth and Planetary Science Letters 436, 56–63.
Dearing Crampton-Flood, E., Tierney, J.E., Peterse, F., Kirkels, F.M.S.A., Sinninghe Damsté, J.S., 2020. BayMBT: A Bayesian calibration model for branched glycerol dialkyl glycerol tetraethers in soils and peats. Geochimica et Cosmochimica Acta 268, 142–159.
Dearing Crampton-Flood, E., van der Weijst, C.M.H., van der Molen, G., Bouquet, M., Yedema, Y., Donders, T.H., Sangiorgi, F., Sluijs, A., Sinninghe Damsté, J.S., Peterse, F., 2021. Identifying marine and freshwater overprints on soil-derived branched GDGT temperature signals in Pliocene Mississippi and Amazon River fan sediments. Organic Geochemistry 154, 104200.
Duan, Y., Sun, Q., Werne, J.P., Hou, J., Yang, H., Wang, Q., Khormali, F., Chen, F., 2022. The impact of precipitation on the distributions of branched tetraethers in alkaline soils. Organic Geochemistry 169, 104410.
Halamka, T.A., Raberg, J.H., McFarlin, J.M., Younkin, A.D., Mulligan, C., Liu, X.-L., Kopf, S.H., 2022. Production of diverse brGDGTs by Acidobacterium *Solibacter usitatus* in response to temperature, pH, and O_2 provides a culturing perspective on brGDGT proxies and biosynthesis. Geobiology 21, 102–118.
Halffman, R., Lembrechts, J., Radujković, D., De Gruyter, J., Nijs, I., De Jonge, C., 2022. Soil chemistry, temperature and bacterial community composition drive brGDGT distributions along a subarctic elevation gradient. Organic Geochemistry 163, 104346.
Harris, C.R., Millman, K.J., van der Walt, S.J., Gommers, R., Virtanen, P., Cournapeau, D., Wieser, E., Taylor, J., Berg, S., Smith, N.J., Kern, R., Picus, M., Hoyer, S., van Kerkwijk, M.H., Brett, M., Haldane, A., del Río, J.F., Wiebe, M., Peterson, P., Gérard-Marchant, P., Sheppard, K., Reddy, T., Weckesser, W., Abbasi, H., Gohlke, C., Oliphant, T.E., 2020. Array programming with NumPy. Nature 585, 357–362.
Hopmans, E.C., Schouten, S., Sinninghe Damsté, J.S., 2016. The effect of improved chromatography on GDGT-based palaeoproxies. Organic Geochemistry 93, 1–6.
Kusch, S., Winterfeld, M., Mollenhauer, G., Höfle, S.T., Schirrmeister, L., Schwamborn, G., Rethemeyer, J., 2019. Glycerol dialkyl glycerol tetraethers (GDGTs) in high latitude Siberian permafrost: Diversity, environmental controls, and implications for proxy applications. Organic Geochemistry 136, 103888.
Lindberg, K.R., Daniels, W.C., Castañeda, I.S., Brigham-Grette, J., 2022. Biomarker proxy records of Arctic climate change during the Mid-Pleistocene transition from Lake El'gygytgyn (Far East Russia). Climate of the Past 18, 559–577.
Martin, C., Ménot, G., Thouveny, N., Davtian, N., Andrieu-Ponel, V., Reille, M., Bard, E., 2019. Impact of human activities and vegetation changes on the tetraether sources in Lake St Front (Massif Central, France). Organic Geochemistry 135, 38–52.
Martínez-Sosa, P., Tierney, J.E., Meredith, L.K., 2020. Controlled lacustrine microcosms show a brGDGT response to environmental perturbations. Organic Geochemistry 145, 104041.
Martínez-Sosa, P., Tierney, J.E., Stefanescu, I.C., Dearing Crampton-Flood, E., Shuman, B.N., Routson, C., 2021. A global Bayesian temperature calibration for lacustrine brGDGTs. Geochimica et Cosmochimica Acta 305, 87–105.
Melles, M., Brigham-Grette, J., Minyuk, P.S., Nowaczyk, N.R., Wennrich, V., DeConto, R. M., Anderson, P.M., Andreev, A.A., Coletti, A., Cook, T.L., Haltia-Hovi, E., Kukkonen, M., Lozhkin, A.V., Rosén, P., Tarasov, P., Vogel, H., Wagner, B., 2012. 2.8 million years of Arctic climate change from Lake El'gygytgyn, NE Russia. Science 337, 315–320.
Muñoz, S.E., Porter, T.J., Bakkelund, A., Nusbaumer, J., Dee, S.G., Hamilton, B., Giosan, L., Tierney, J.E., 2020. Lipid biomarker record documents hydroclimatic variability of the Mississippi River Basin during the Common Era. Geophysical Research Letters 47. https://doi.org/10.1029/2020GL087237.
Muñoz-Sabater, J., 2021. ERA5-Land monthly averaged data from 1950 to 1980. Copernicus Climate Change Service (C3S) Climate Data Store (CDS). [WWW Document]. URL (accessed 12.1.21).
Naafs, B.D.A., Gallego-Sala, A.V., Inglis, G.N., Pancost, R.D., 2017a. Refining the global branched glycerol dialkyl glycerol tetraether (brGDGT) soil temperature calibration. Organic Geochemistry 106, 48–56.
Naafs, B.D.A., Inglis, G.N., Zheng, Y., Amesbury, M.J., Biester, H., Bindler, R., Blewett, J., Burrows, M.A., del Castillo Torres, D., Chambers, F.M., Cohen, A.D., Evershed, R.P., Feakins, S.J., Gałka, M., Gallego-Sala, A., Gandois, L., Gray, D.M., Hatcher, P.G., Honorio Coronado, E.N., Hughes, P.D.M., Huguet, A., Könönen, M., Laggoun-Défarge, F., Lähteenoja, O., Lamentowicz, M., Marchant, R., McClymont, E., Pontevedra-Pombal, X., Ponton, C., Pourmand, A., Rizzuti, A.M., Rochefort, L., Schellekens, J., De Vleeschouwer, F., Pancost, R.D., 2017b. Introducing global peat-specific temperature and pH calibrations based on brGDGT bacterial lipids. Geochimica et Cosmochimia Acta 208, 285–301.
Naafs, B.D.A., Oliveira, A.S.F., Mulholland, A.J., 2021. Molecular dynamics simulations support the hypothesis that the brGDGT paleothermometer is based on homeoviscous adaptation. Geochimica et Cosmochimica Acta 312, 44–56.
Naafs, B.D.A., Rohrssen, M., Inglis, G.N., Lähteenoja, O., Feakins, S.J., Collinson, M.E., Kennedy, E.M., Singh, P.K., Singh, M.P., Lunt, D.J., Pancost, R.D., 2018. High temperatures in the terrestrial mid-latitudes during the early Palaeogene. Nature Geoscience 11, 766.
Otiniano, G.A., Porter, T.J., Benowitz, J.A., Bindeman, I.N., Froese, D.G., Jensen, B.J.L., Davies, L.J., Phillips, M.A., 2020. A Late Miocene to Late Pleistocene reconstruction of precipitation isotopes and climate from hydrated volcanic glass shards and biomarkers in central Alaska and Yukon. Paleoceanography and Paleoclimatology 35. https://doi.org/10.1029/2019PA003791.
Peltier, C., 2015. Application of the Branched Glycerol Dialkyl Glycerol Tetraether (brGDGT) Temperature Proxy on Tropical Lake Bosumtwi in West Africa: Assessment of the Proxy and the Resulting 2,000 Year Paleotemperature Record, Mount Holyoke College Thesis.
Raberg, J.H., Flores, E., Crump, S.E., de Wet, G., Dildar, N., Miller, G.H., Geirsdóttir, Á., Sepúlveda, J., 2022a. Intact polar brGDGTs in Arctic lake catchments: Implications for lipid sources and paleoclimate applications. Journal of Geophysical Research: Biogeosciences 127, e2022JG006969.
Raberg, J.H., Harning, D.J., Crump, S.E., de Wet, G., Blumm, A., Kopf, S., Geirsdóttir, Á., Miller, G.H., Sepúlveda, J., 2021. Revised fractional abundances and warm-season temperatures substantially improve brGDGT calibrations in lake sediments. Biogeosciences 18, 3579–3603.
Raberg, J.H., Miller, G.H., Geirsdóttir, Á., Sepúlveda, J., 2022b. Near-universal trends in brGDGT lipid distributions in nature. Science Advances 8, eabm7625.
Reback, J., Mendel, J.B. McKinney, W., Van Den Bossche, J., Roeschke, M., Augspurger, T., Hawkins, S., Cloud, P., Young, G.F., Hoefler, P., Sinhrks, Klein, A., Petersen, T., Tratner, J., She, C., Ayd, W., Shadrach, R., Naveh, S., Garcia, M., Darbyshire, J.H.M., Schendel, J., Wörtwein, T., Hayden, A., Saxton, D., Gorelli, M.E., Li, F., Zeitlin, M., Jancauskas, V., McMaster, A., Li, T., 2022. pandas-dev/pandas: Pandas 1.4.4. doi: 10.5281/ZENODO.3509134.
Russell, J.M., Hopmans, E.C., Loomis, S.E., Liang, J., Sinninghe Damsté, J.S., 2018. Distributions of 5- and 6-methyl branched glycerol dialkyl glycerol tetraethers (brGDGTs) in East African lake sediment: Effects of temperature, pH, and new lacustrine paleotemperature calibrations. Organic Geochemistry 117, 56–69.
Salvatier, J., Wiecki, T.V., Fonnesbeck, C., 2016. Probabilistic programming in Python using PyMC3. PeerJ Computer Science 2, e55.
Sinninghe Damsté, J.S., Rijpstra, W.I.C., Foesel, B.U., Huber, K.J., Overmann, J., Nakagawa, S., Kim, J.J., Dunfield, P.F., Dedysh, S.N., Villanueva, L., 2018. An overview of the occurrence of ether- and ester-linked *iso*-diabolic acid membrane lipids in microbial cultures of the Acidobacteria: Implications for brGDGT paleoproxies for temperature and pH. Organic Geochemistry 124, 63–76.
Sinninghe Damsté, J.S.S., Hopmans, E.C., Pancost, R.D., Schouten, S., Geenevasen, J.A.J., 2000. Newly discovered non-isoprenoid glycerol dialkylglycerol tetraether lipids in sediments. Chemical Communications 2000, 1683–1684.
Sinninghe Damsté, J.S.S., Rijpstra, W.I.C., Hopmans, E.C., Weijers, J.W.H., Foesel, B.U., Overmann, J., Dedysh, S.N., 2011. 13,16-Dimethyl octacosanedioic acid (*iso*-diabolic acid), a common membrane-spanning lipid of Acidobacteria Subdivisions 1 and 3. Applied and Environmental Microbiology 77, 4147–4154.
Stefanescu, I.C., Shuman, B.N., Tierney, J.E., 2021. Temperature and water depth effects on brGDGT distributions in sub-alpine lakes of mid-latitude North America. Organic Geochemistry 152, 104174.
Tierney, J.E., Tingley, M.P., 2018. BAYSPLINE: A New Calibration for the Alkenone Paleothermometer. Paleoceanography and Paleoclimatology 33, 281–301.
van Bree, L.G.J., Peterse, F., Baxter, A.J., De Crop, W., van Grinsven, S., Villanueva, L., Verschuren, D., Sinninghe Damsté, J.S., 2020. Seasonal variability and sources of in situ brGDGT production in a permanently stratified African crater lake. Biogeosciences 17, 5443–5463.
Véquaud, P., Thibault, A., Derenne, S., Anquetil, C., Collin, S., Contreras, S., Nottingham, A.T., Sabatier, P., Werne, J.P., Huguet, A., 2022. FROG: A global machine-learning temperature calibration for branched GDGTs in soils and peats. Geochimica et Cosmochimica Acta 318, 468–494.
Virtanen, P., Gommers, R., Oliphant, T.E., Haberland, M., Reddy, T., Cournapeau, D., Burovski, E., Peterson, P., Weckesser, W., Bright, J., van der Walt, S.J., Brett, M., Wilson, J., Millman, K.J., Mayorov, N., Nelson, A.R.J., Jones, E., Kern, R., Larson, E., Carey, C.J., Polat, İ., Feng, Y., Moore, E.W., VanderPlas, J., Laxalde, D., Perktold, J.,

Cimrman, R., Henriksen, I., Quintero, E.A., Harris, C.R., Archibald, A.M., Ribeiro, A. H., Pedregosa, F., van Mulbregt, P., 2020. SciPy 1.0 Contributors, SciPy 1.0: fundamental algorithms for scientific computing in Python. Nature Methods 17, 261–272.

Wang, H., Chen, W., Zhao, H., Cao, Y., Hu, J., Zhao, Z., Cai, Z., Wu, S., Liu, Z., Liu, W., 2023. Biomarker-based quantitative constraints on maximal soil-derived brGDGTs in modern lake sediments. Earth and Planetary Science Letters 602, 117947.

Wang, M., Zong, Y., Zheng, Z., Man, M., Hu, J., Tian, L., 2018. Utility of brGDGTs as temperature and precipitation proxies in subtropical China. Scientific Reports 8, 194.

Weber, Y., Sinninghe Damsté, J.S., Zopfi, J., De Jonge, C., Gilli, A., Schubert, C.J., Lepori, F., Lehmann, M.F., Niemann, H., 2018. Redox-dependent niche differentiation provides evidence for multiple bacterial sources of glycerol tetraether lipids in lakes. Proceedings of the National Academy of Sciences USA 115, 10926–10931.

Weijers, J.W., Schouten, S., Hopmans, E.C., Geenevasen, J.A.J., David, O.R.P., Coleman, J.M., Pancost, R.D., Sinninghe Damsté, J.S., 2006. Membrane lipids of mesophilic anaerobic bacteria thriving in peats have typical archaeal traits. Environmental Microbiology 8, 648–657.

Weijers, J.W., Schouten, S., van den Donker, J.C., Hopmans, E.C., Sinninghe Damsté, J. S., 2007. Environmental controls on bacterial tetraether membrane lipid distribution in soils. Geochimica et Cosmochimica Acta 71, 703–713.

Willard, D.A., Donders, T.H., Reichgelt, T., Greenwood, D.R., Sangiorgi, F., Peterse, F., Nierop, K.G.J., Frieling, J., Schouten, S., Sluijs, A., 2019. Arctic vegetation, temperature, and hydrology during Early Eocene transient global warming events. Global and Planetary Change 178, 139–152.

Wu, J., Yang, H., Pancost, R.D., Naafs, B.D.A., Qian, S., Dang, X., Sun, H., Pei, H., Wang, R., Zhao, S., Xie, S., 2021. Variations in dissolved O2 in a Chinese lake drive changes in microbial communities and impact sedimentary GDGT distributions. Chemical Geology 579, 120348.

Xiao, W., Wang, Y., Zhou, S., Hu, L., Yang, H., Xu, Y., 2016. Ubiquitous production of branched glycerol dialkyl glycerol tetraethers(brGDGTs) in global marine environments: a new source indicator for brGDGTs. Biogeosciences 13, 5883–5894.

Zhao, B., Castañeda, I.S., Bradley, R.S., Salacup, J.M., de Wet, G.A., Daniels, W.C., Schneider, T., 2021. Development of an in situ branched GDGT calibration in Lake 578, southern Greenland. Organic Geochemistry 152, 104168.